TD-08-025

v. 6 Sept. 26, 2008

L-Band, Waveguide-Based, Fast, High Power Phase Shifter

T. Khabiboulline, N. Solyak, I. Terechkine

I. Introduction

After test results of a CW prototype of an L-band, ferrite loaded waveguide-based phase shifter [1] were analyzed, a set of factors limiting the shifter performance were identified in [2] and ways to improve the performance were proposed. Each limiting factor resulted in appearance of a resonant mode coupled with the main TE_{10} mode. Some of the factors, like symmetry in the ferrite block positioning, were easy to eliminate by using tight dimensional tolerances and appropriate assembly tooling. Other important limitations included non-uniformity of magnetic properties of the ferrite blocks, some difference in bias field of the blocks, and imperfect matching of the ferrite-loaded section of the phase shifter waveguide. To make a reliable device that could be used in an RF distribution system of an accelerator, we must neutralize factors that lead to the appearance of the resonances. The device must also meet the fast phase change rate requirement. Besides, the ferrite blocks must be protected from excessive heating, which would otherwise lead to deterioration of the device properties.

The next measures help to improve the performance of the phase shifter:

- local reduction of the waveguide width increases the cut-off frequency of TE_{20} modes;
- reduction of the waveguide height helps to eliminated conditions for excitation of TE_{11} mode. This measure also helps to simplify the magnetic system of the device;
- using thinner ferrite blocks leads to lower bias field and simplifies heat management;

Keeping these measures in mind, we also need to think about future integration of the device into a fast, high power vector modulator that regulates phase and amplitude of RF power directed into cavities of a linear accelerator. Besides the phase shift range and maximum power handled by the device, one needs to care about the phase change rate of the device, which is not always a trivial task for waveguide-based systems.

Next sections of the note describe a design concept of a phase shifter that can serve as a base element of the vector modulator for use in the RF power distribution system of linear accelerators. Following schematic description of the device, the next features will be detailed:

- expected RF properties of the device, including phase shift range and power handling capability;
- waveguide design features that ensure fast penetration of the pulsed magnetic field inside the ferrite blocks;
- magnetic bias system design concept, including static bias field circuit and pulsed magnetic field circuit;
- some considerations about choosing a power supply;

II. Main design features of the phase shifter

Fig. 1 shows main features of the proposed phase shifter. Two blocks of Yttrium Iron Garnet (YIG) of rectangular cross-section are placed inside a rectangular waveguide in close contact with the side walls. Heat generated in the blocks is removed by cooling the walls. The height of the waveguide is chosen to ensure propagation of required RF

power in the waveguide. On the other hand, this height dictates design features of a magnetic bias circuit of the device. There are two main components in the magnetic bias: a permanent bias and a fast bias. The permanent bias is created by using permanent magnets with the help of pole pieces and flux return blocks. The direction of this bias field is opposite in the two YIG blocks. To excite the pulsed component of the bias field, fast bias windings are used. If the permanent magnet blocks and the pulsed windings share the same magnetic circuit, spatial shape of the bias field in the absence of the waveguide is essentially the same for the static and dynamic magnetic field components. Eddy currents in the walls of the waveguide redirect the fast component of the magnetic field and special design measures are needed to ensure field penetration inside the waveguide; this issue will be discussed later in this note. To handle both the static and pulsed bias field, the pole pieces and the flux return blocks must be made of soft magneto-ceramic.

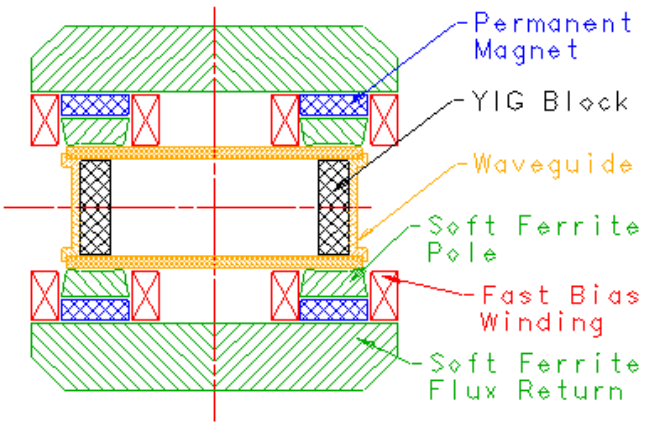

Fig. 1: Concept of the high power fast phase shifter

While choosing permanent magnet material, we need to take into account two factors:

- First, the magnets must create needed static bias field in the YIG blocks. Meeting this goal by using stronger (and hence thinner) magnets relaxes requirements for the pulsed excitation system, including the power supply.

- On the other hand, the strongest permanent magnet materials like SmCo or FeB_2 are metal alloys. Having high electric conductivity, they can significantly deform the pulsed magnetic field spatial shape; so, the design of the pulsed circuit must take into account eddy currents in the permanent magnet blocks.

Understanding challenges of the phase shifter design, we can now start systematic description of its components. Obviously, the main part of the device is YIG block-loaded waveguide.

III. Ferrite-loaded waveguide

The design used in [1] was significantly modified. Our goal was to eliminate (or at least to neutralize or mitigate) main factors that limited the high power performance of that device. The 2-MW design had several trapped RF modes within the operating frequency range. To move TE_{11n} resonances out of this range (towards higher frequencies), the waveguide height of 36 mm was chosen. Width of the YIG loaded waveguide was also reduced to move TE_{20n} resonances to higher frequencies. Transition section from regular WR650 waveguide to the ferrite-loaded section of the waveguide

was configured taking into account minimization of reflection from the transition and providing additional space for the windings of the fast bias magnetic system. The ferrite blocks were made 11 mm thick. Although followed by some reduction of the phase shift range, this measure resulted in elimination of several unwanted RF modes and simplified the heat removal from the blocks. Schematic view of the waveguide is shown in Fig. 2.

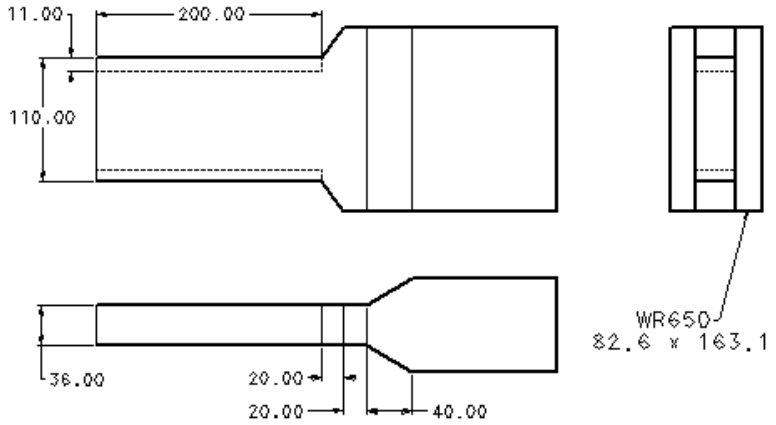

Fig. 2: Ferrite-loaded waveguide of the phase shifter

Electrical, magnetic and RF properties of YIG material used during modeling are listed in a table below and correspond to that of G-510 aluminum-doped YIG blocks by Trans-Tech, Inc. that we used in our previous work [1]. Changes to some parameter values were made to better reflect results of our in-house material test.

Table 1. Electromagnetic parameters of YIG material

Saturation magnetization ($4\pi M_S$) @ 23 (Gs)	550 ± 5%
Lande g-factor	2.01
Line width at 1.3 GHz at -3dB (Gs)	4
Dielectric Constant at 1.3 GHz and -3 dB	13.76
Dielectric Loss Tangent tan(δ) at 1.3 GHz	$5*10^{-5}$
Curie Temperature (°C)	155
Initial Permeability μ @ 1 kHz	37
Saturation Induction Bm @ H = 5 Oe (Gs)	450
Remanent Induction B*r* (Gs)	398
Coercive Force H*c* (Oe)	0.55

The material properties depend on temperature. Although temperature related changes of the phase shifter performance were not studied yet, this study needs to be made later. For the benefit of this future study, we summarize known data about changes of YIG material properties with the temperature in Table 2.

Table 2: Thermal coefficients @ 25°C

Saturation magnetization k_{SM} (Gs / °C)	- 1.1
Remanent Induction k_{Br} (Gs / °C)	-1.2
Coercive Force Hc (Oe / °C)	-0.003

Three versions of the ferrite-loaded waveguide with the widths 100 mm, 110 mm, and 120 mm were analyzed. First a wave transition analysis (no shortened end) was made of the two-port system shown in Fig. 3.

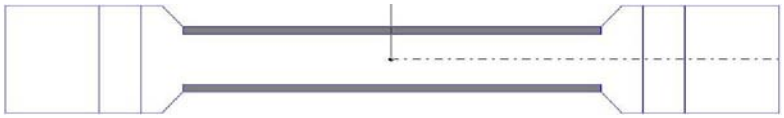

Fig. 3: Waveguide width optimization configuration

In Fig.4, Fig.5, and Fig.6, transition coefficients S21 are shown for each waveguide width in the frequency range between 1.1 GHz and 1.5 GHz for symmetric and shifted vertical positioning of the YIG blocks and for anti-symmetric and unbalanced magnetic bias field. For a waveguide with ideally placed and biased ferrites (bias field is 700 Gs), better matching with regular WG and acceptable frequency range was reached in the version with 100 mm and 110 mm waveguide width (Fig. 4).

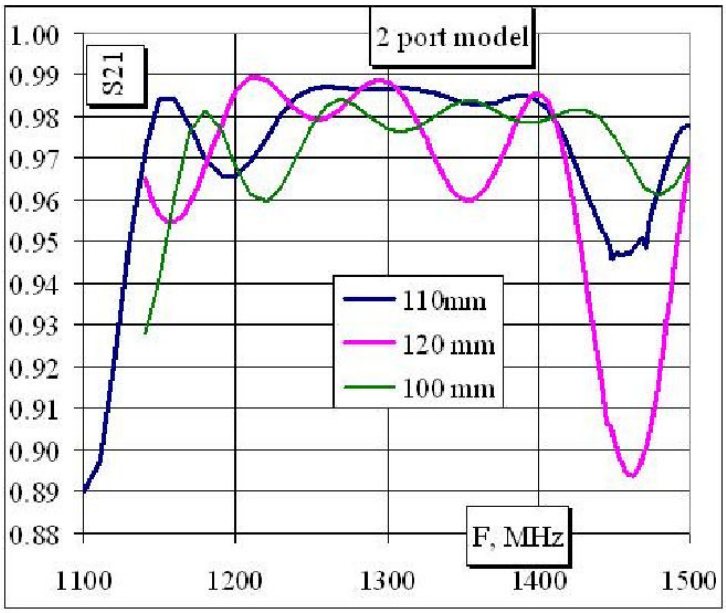

Fig. 4: Ferrite-loaded waveguide width choice. Ferrite block are positioned symmetrically. Equal magnetic field of 700 Gs in the two blocks.

Fig. 5 illustrates the case when the magnetic bias in one block is 20 Gs higher than that in another. Both blocks are vertically centered in the waveguide. Resonances can be seen with frequencies higher than the operating frequency (1300 MHz). With low bias field, significant resonance effects take place in the vicinity of the operating frequency. By increasing the bias, the resonances can be made weaker; it is not noticeable at the bias

of 700 Gs. This low sensitivity of the RF transfer function to asymmetry of the bias field is the main reason of why the 700 Gs level of the bias was accepted for future study.

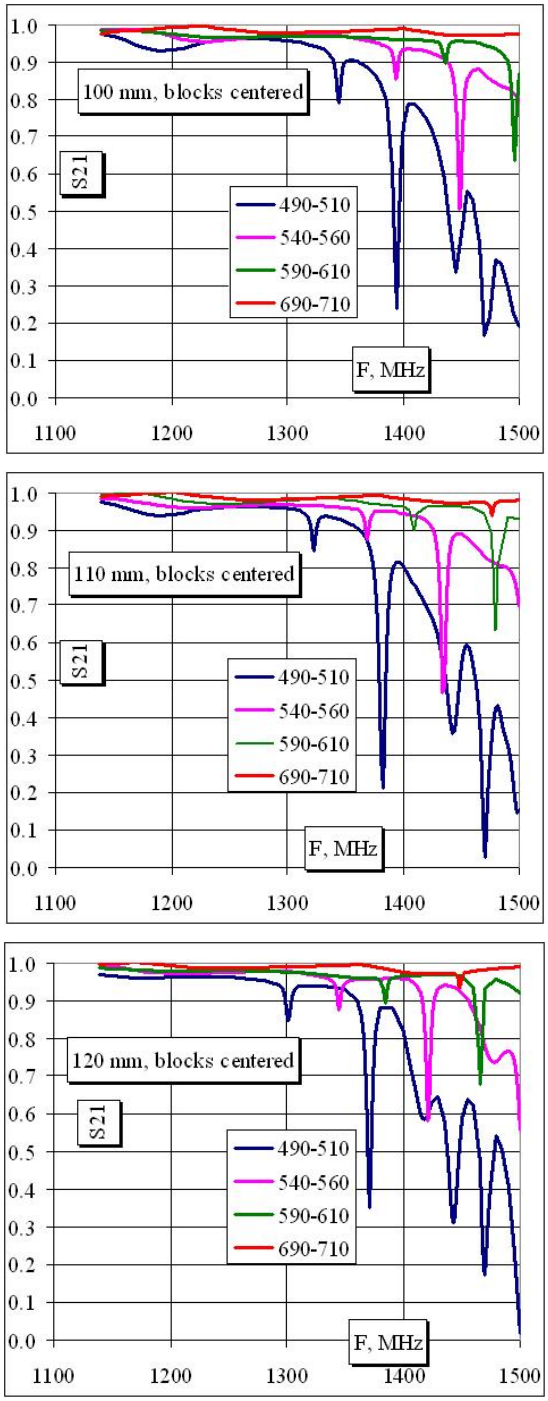

Fig. 5: Ferrite-loaded waveguide width choice. Ferrite block are centered vertically. Magnetic field in the two blocks is unbalanced.

Geometrical asymmetry in the vertical positioning of the blocks also results in the appearance of resonances. Fig. 6 below compares reflected wave diagrams in cases when

the ferrite blocks are shifted from their center position and magnetic bias field in one of the blocks differs from that in another.

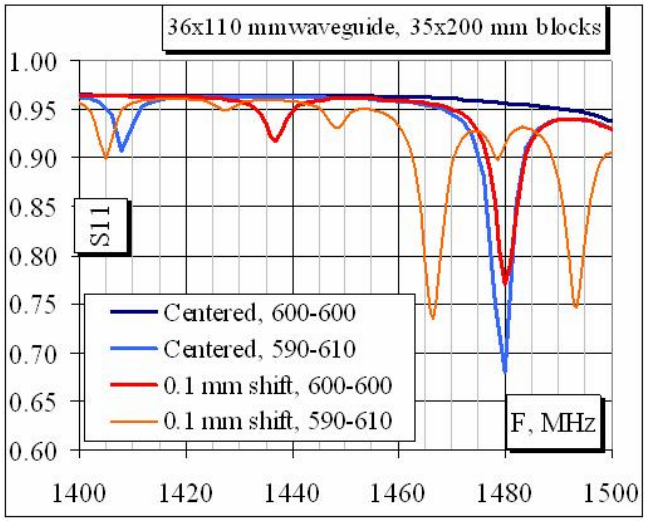

Fig. 6: Ferrite-loaded waveguide width choice. Resonances due to the vertical shift of the ferrite blocks and/or unbalanced magnetic bias.

When the ferrite blocks are centered vertically and anti-symmetric bias field is applied, there are no visible resonances in the frequency range of interest (black curve: centered, 600-600; the numbers show magnetic field in Gauss in the blocks). Bias asymmetry results in the appearance of two resonances: TE_{201} at 1407 MHz and TE_{202} at 1479 MHz (blue curve: centered, 690-610). Vertical shift by 0.1mm in the same direction of equally biased blocks also results in the appearance of two resonances: TE_{111} at 1437 MHz and TE_{112} at 1480 MHz (red curve: 0.1 mm shift, 600-600). The bias asymmetry of 20 Oe applied to the shifted blocks splits these two modes; now in the frequency range between 1.4 GHz and 1.5 GHz six resonances are observed: one TE_{201} mode, two TE_{111} modes (one for each block), one TE_{202}, and two TE_{112} modes (light brown curve 0.1 mm shift, 590-610). As it was notices for the asymmetry of the bias, the effect of the asymmetry in the block positioning is more pronounced for lower bias field.

Fig. 7 shows phase change and reflective wave power loss diagrams at the operation frequency in the magnetic bias field range from 500 Gs to 1300 Gs.

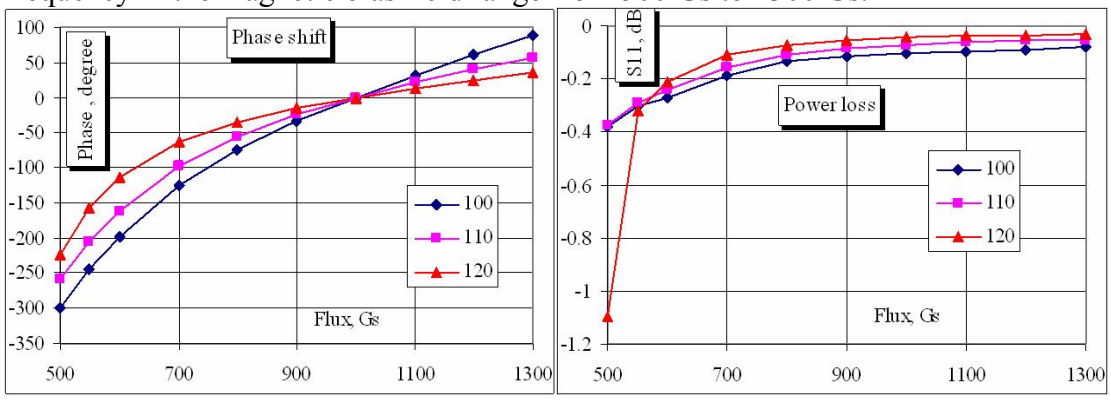

a) b)

Fig. 7: Phase change range in degrees (a) and power loss in dB (b). Magnetic field is in Gs in this graph.

While the system with the waveguide width of 100 mm provides smoother and larger phase change, power loss are minimal in the system with 120 mm wide waveguide. The choice of the system with 110 mm waveguide width is a quite reasonable compromise. This configuration can provide phase shift of ~200° when bias field changes from 500 Gs to 900 Gs. With the central bias of 700 Gs, pulsed magnetic system must provide ±200 Gs shift of the bias point.

IV. Power handling capability

Two factors must be taken into account while trying to define the ultimate power the device can handle: the heating of the YIG blocks and sparking in the ferrite-loaded section of the waveguide. Requirements to the device naturally depend on the power requirements to a linac that will be using the devices. Besides, an optimal thermal design can be made only when details of phase shift algorithm are known.

The input RF power of a multi-cell elliptical cavity of a high energy superconducting linac is ~250 kW. As it was pointed out in [7], the most reliable scheme of connection of a vector modulator in the RF distribution line is separating it from the cavity by a directional insulator (or by a circulator). In this case, each branch of the vector modulator sees a half of the total power, that is ~125 kW.

Electromagnetic properties of each YIG block of the phase shifter will depend on its temperature, which is not uniform through the block. As it was mentioned above, this temperature depends also on the way the phase shifter is used. Although many details are not clear at the moment, we can make an evaluation of the block temperature based on the average RF power passing through.

Because a shorted waveguide is employed in our case, a standing wave is established in the blocks in the direction of the waveguide length with ~100% wave amplitude modulation. In the horizontal direction across the waveguide, the presence of the ferrites makes the field distribution even more complicated. Even in the vertical direction the field is not uniform due to the presence of gaps between the ferrite blocks and the walls of the waveguide. We will refer to the longitudinal coordinate as X, to the horizontal transverse direction as Y, and to the vertical transverse direction as Z.

As it is shown in Table 1 of this note, the dielectric loss tangent of the YIG material is very low, so power loss is mainly due to the changing magnetic field (hysteretic and resistive components). Because the working point of the material in the phase shifter is in the saturated part of magnetization curve, we have mainly resistive losses and quadratic dependence of the losses on the magnetic field strength.

Fig. 8 shows magnetic field distribution in the ferrite loaded waveguide with the input power of 1 Watt. The vertical directions in this figure is along the length of the waveguide (X direction). The horizontal direction is Y in the left part and Z in the right part of the figure; these are the directions in the plane of the waveguide cross-section. There is a shorted end at the top part of the waveguide (as shown), and there is transition to the regular WR650 waveguide at the bottom part.

Magnetic field within the YIG block can be approximated using the next expression:

$$H = H_m \cdot \cos\frac{2\pi}{\lambda_X}(X - X_m) \cdot \cos\frac{2\pi}{\lambda_Y}(Y - Y_m) \cdot \cos\frac{2\pi}{\lambda_Z}(Z - Z_m) \qquad (1)$$

with parameters defined in Table 3. The change range of X, Y, and Z is defined by the size of the YIG block. In our case, $X \in (0, 200\text{ mm})$, $Y \in (0, 11\text{ mm})$, and $Z \in (0, 35\text{ mm})$.

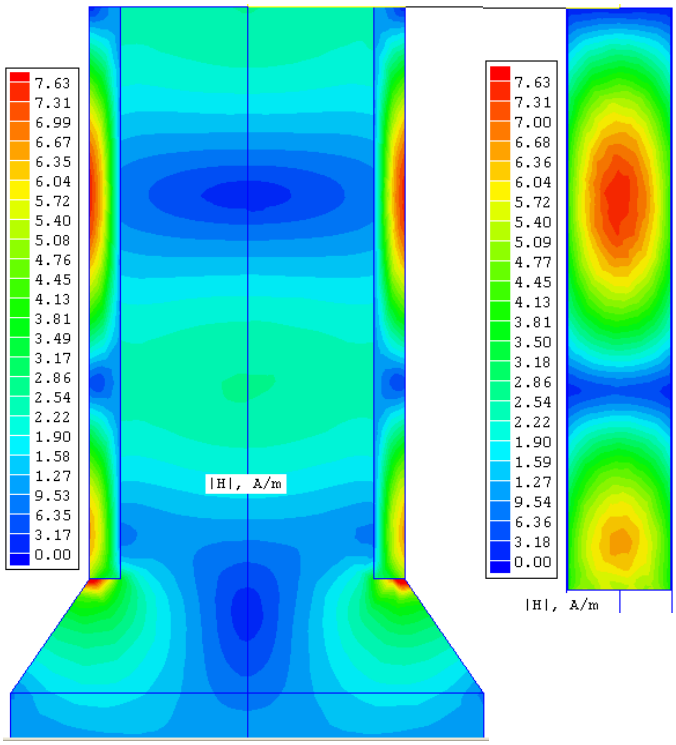

Fig. 8: Magnetic field distribution in ferrite-loaded waveguide with 1 Watt input power.

Table 3: Magnetic field distribution in YIG block at 1 Watt input power

Hm (A/m)	λ_X (m)	Xm (m)	λ_Y (m)	Ym (m)	λ_Z (m)	Zm (m)
7.5	0.262	0.066	0.045	0	0.114	0.018

Because the volumetric power loss is proportional to the square of the magnetic field, we can write:

$$p(X,Y,Z) = A \cdot \left[H_m \cdot \cos\frac{2\pi}{\lambda_X}(X - X_m) \cdot \cos\frac{2\pi}{\lambda_Y}(Y - Y_m) \cdot \cos\frac{2\pi}{\lambda_Z}(Z - Z_m) \right]^2 \ [\mathrm{W/m^3}] \quad (2)$$

Knowing the total power dissipated in the block and integrating (2) through the volume of the block, we can find the coefficient A. Obviously $A \cdot H_m^2 \equiv p_m$.

Power loss in one block is one halve of the loss in the waveguide, which is found by analyzing the reflected wave diagram similar to that in Fig. 5. Average S11 coefficient is 0.982 that corresponds to 3.6% of lost power. So, with 1 W of the phase shifter input power, the maximum power loss **in one block** is $P_{loss\_1W} = 0.036 \cdot 1/2 = 0.018$ W. Now we can find the coefficient A in (2) by performing the integration over the volume of one YIG block. Power loss in one YIG block at 1 W of the input power is

$$P_{loss\_1W} = 0.018 \text{ W} = 1.5 \cdot 10^{-5} \cdot A \cdot (H_{m\_1W})^2.$$

Because we know that $H_{m\_1W} = 7.5$ A/m, coefficient A is

$$A = 21.3 \text{ W/(A/m)}^2/\text{m}^3$$

At different input power,

$$P_{in} / P_{1W} = H_m^2 / (H_{m\_1W})^2$$

and ($P_{1W} = 1$ W)

$$H_m^2 = P_{in} \cdot (H_{m\_1W})^2 = 7.5^2 \cdot P_{in}$$

Expression (1) can be written then in terms of the input power:

$$p(X,Y,Z) = A \cdot 7.5^2 \cdot P_{in} \cdot \left[\cos\frac{2\pi}{\lambda_X}(X - X_m) \cdot \cos\frac{2\pi}{\lambda_Y}(Y - Y_m) \cdot \cos\frac{2\pi}{\lambda_Z}(Z - Z_m) \right]^2 \text{[W/m}^3\text{]} \quad (3)$$

With the input power of the Vector Modulator (which contains two phase shifters) of 250 kW, P_{in} = 125 kW, and the maximum volumetric power loss in one YIG block will be ~ $1.5*10^8$ W/m^3 or 150 W/cm^3. The total thermal load for one block will be ~ 1.8% of the input power or ~ 2250 W. The maximum temperature of the YIG blocks will be defined by a filling factor of accelerator RF system and by thermal conductivity of the ferrite material. Material properties relevant to the heating process are shown in Table 4

Table 4: Relevant properties of YIG material

Property	Unit	Value
Thermal conductivity	W/(m·K)	7.4
Specific heat	kJ/(kg·K)	4.5
Specific weight	kg/m^3	5170

Fig. 9 below shows the power deposition in the block with the maximum power density of $5*10^6$ W/m^3, which corresponds to the maximum RF power per one phase shifter of 125 kW and the RF system filling factor of ~ 3.3%. Corresponding temperature distribution is also shown in Fig. 9. The temperature rise in the hottest spot is ~10 K, which we consider quite acceptable.

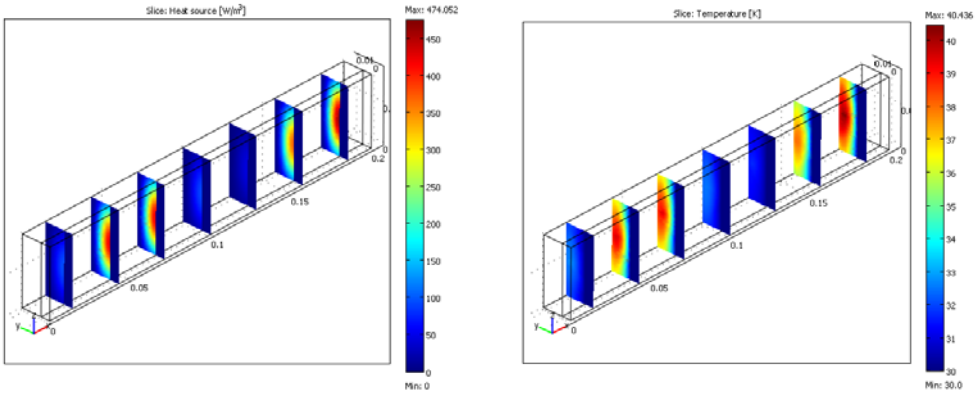

a) b)

Fig. 9: Power deposition (a) and temperature distribution (b) in the ferrite block

It is also useful to know what time it takes for the block to reach the stage of static temperature distribution. Corresponding graph for the hottest spot is shown in Fig. 10.

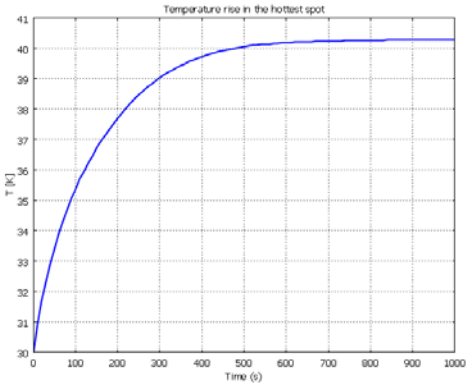

Fig. 10: Temperature rise in the hottest spot of the YIG block.

Time constant of the heating process is ~ 200 seconds or ~ 3 minutes.

Another limiting factor in the power handling capability of the device is sparking. Our previous experience with the sparking forced us to consider trapezoidal shape of the YIG blocks. Other solutions include encapsulation of the block in polyethylene (or other low power loss, high dielectric strength media) to ensure the absence of a gap between the top of the block and the wall of the waveguide or using SF_6 gas to fill the waveguide. Without this measure, in our case, at the input power of 125 kW, the electric field in the 0.5-mm air gap between the YIG block and the waveguide wall reaches ~22.5 kV, which seems acceptable.

As a conclusion for this section, we can state that the suggested configuration of the phase shifter can provide power handling capability well suited for use in a vector modulator needed in a RF power distribution circuit of a linac.

IV. Waveguide design concept

As it was mentioned earlier, it is very important to design the ferrite loaded waveguide of the phase shifter so that the pulsed magnetic field could penetrate into the YIG blocks. Walls of standard copper-made waveguides (~ 2 mm thick), although transparent for static magnetic field, loose their transparency at frequency increases due to eddy currents in the walls. Fig. 11 shows modeling geometry with eddy current density in the walls of the waveguide at 1000 Hz. Magnetic field penetration efficiency in the frequency range from 0.1 Hz to 1000 Hz. is shown on the right of the figure; the same excitation current density was used for all the frequencies.

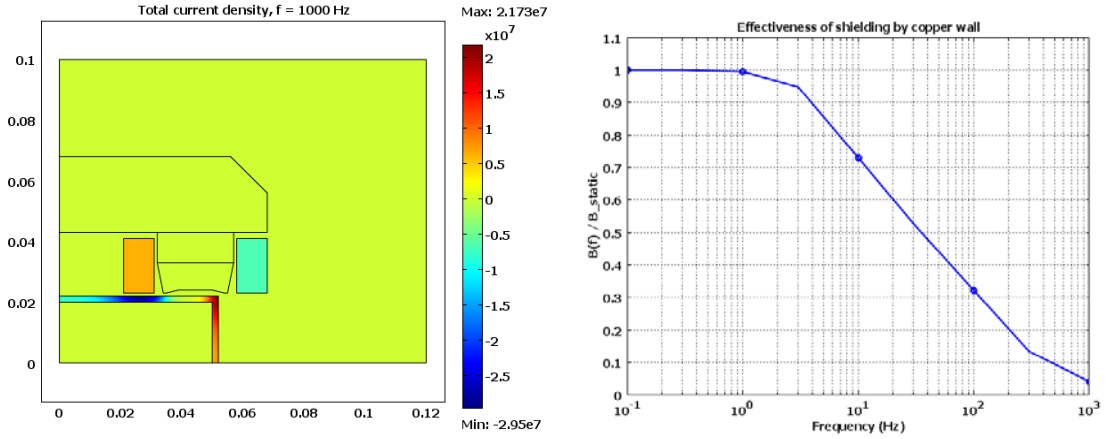

a) b)

Fig. 11. Modeling geometry (a) and magnetic field shielding efficiency (b) by a waveguide with 2-mm thick copper walls.

The magnetic field penetrates well (transition better that 90%) only when the frequency is below ~4 Hz. Although here we do not see very pronounced skin effect even at 1000 Hz (the skin depth for copper at 1000 Hz is ~2.2 mm), the field is very effectively shielded by the waveguide.

Making the walls made of stainless steel helps, but not solves the problem (Fig. 12). Now the shielding works well starting with the frequency $f \approx 100$ Hz. This frequency range corresponds to the response time of ~5 ms.

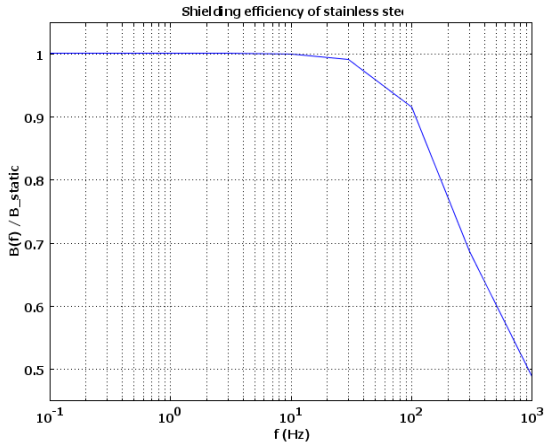

Fig. 12. Magnetic field shielding efficiency by walls of a waveguide made of 2-mm stainless steel.

What material and what thickness should be used depends on required frequency response of the system. Fig. 13 shows shielding efficiency for the waveguide in Fig. 11-a with the wall thickness characterized by different values of the surface resistance.

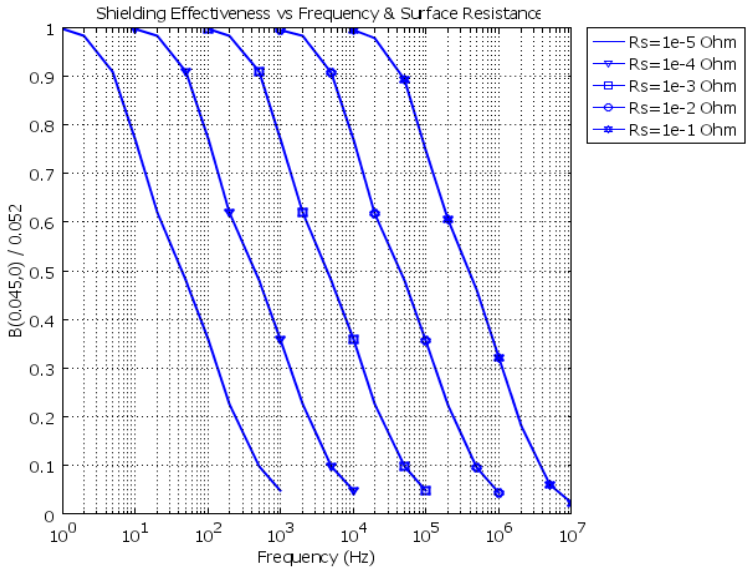

Fig. 13: Effectiveness of penetration of magnetic field inside waveguide formed by conductor coated dielectric walls. Parameter of the coating is surface resistance Rs.

Effective skin layer for copper at the operation frequency of 1.3 GHZ is ~ 1.84 μm. Wall thickness must be several times this value to limit the RF power radiation through the walls. The smallest thickness we can use without seriously increasing power loss through radiation is ~5 μm (this is consistent with the statement made in [4]). This corresponds to the surface resistance Rs = $4*10^{-3}$ Ohm. So, our choice of the thickness is limited by performance of the waveguide. Frequency response for the system with 5 μm thick, copper waveguide is shown in Fig. 14-a. Transient properties of the same system are shown in Fig. 14-b where the magnetic system is excited by a rectangular current pulse and the magnetic field inside the waveguide is measured. The field penetration time constant is ~40 μs, which agrees well with the frequency response that shows the cut-off ~10 kHz.

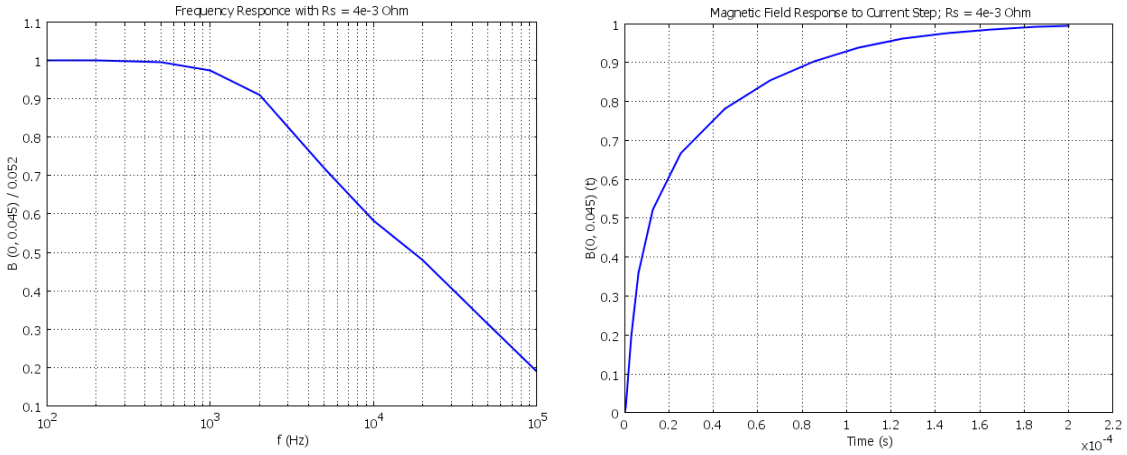

a) b)

Fig. 14: Shielding effectiveness (a) and transient properties (b) of the waveguide with the wall thickness of 5 μm (surface resistance Rs = $4*10^{-3}$ Ohm)

Further improvements can be made by adjusting the shape of the excitation current to effectively reduce the time constant by applying higher current rise rate in the beginning of the pulse.

Not every part of the waveguide is equal in resisting to magnetic field penetration. Horizontal (top and bottom) walls play the major role here; the thickness of conductive vertical (side) walls is less important. Increased thickness of the side walls can even be somewhat beneficial. To demonstrate this, let's check the magnetic field response in the case similar to the previous, but with thicker (2 mm) copper side wall (Fig. 15).

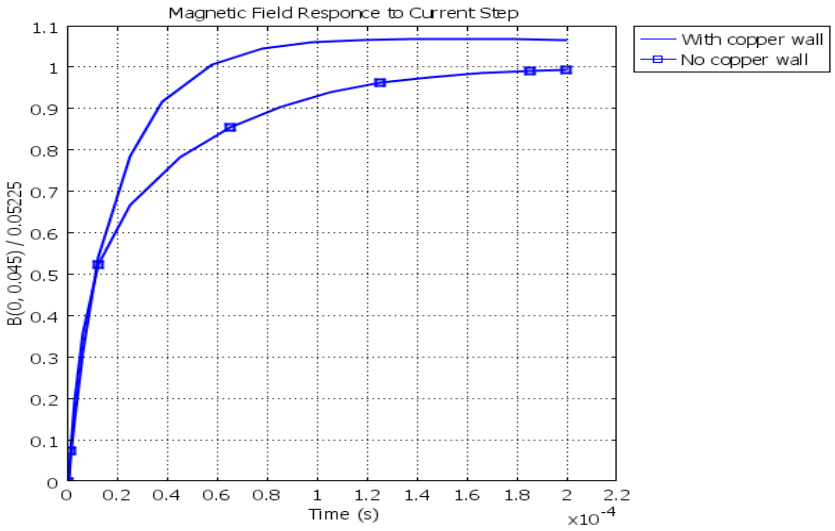

Fig. 15: Magnetic field response with and without thick copper side wall

Response time became almost twice as small in this case because of redistribution of the magnetic field pushed out of the copper side wall. Now field penetration time constant is ~25 μs. This (quite understandable, but unexpected) feature can be helpful while arranging for a heat sink from the YIG blocks to outside of the waveguide. It also helps to form a design concept for the waveguide – relatively thick copper side walls and strong silver coated alumina ceramic plates for the top and bottom.

As it follows from Fig. 7, the average magnetic field swing of ~200 Gs corresponds to the phase shift ~100°. Having in mind the magnetic field change time scale of ~25 μs, we can reach the phase shift rate of ~4°/μs.

As a conclusion to this section, we can say that the ferrite-loaded waveguide can be made by using coated dielectric plates to form the top and bottom of a waveguide (5 μm copper or silver coating results in the required surface resistance of ~$4*10^{-3}$ Ohm) and relatively thick conducting side walls. Good candidate for the top and bottom plates is alumina ceramics. Plates made of 96% or 99.5% alumina are readily available. Several US companies provide controlled coating service. In addition to providing a strong support and a base for coating, due to high permittivity, alumina material also helps to reduce RF power leak through the walls.

V. Permanent Magnet Circuit

In accordance with Fig. 1, the fast bias magnetic field circuit coincides with that of the permanent bias. We need to configure this permanent bias before switching to the pulsed bias.

There are several things to take into account. First, the length in the direction of magnetization of the magnet must be as small as possible because this length will increase the effective air gap of the circuit and result in the need of more ampere-turns in the fast coil. In turn, this will increase the inductance of this circuit leading to longer response time and requiring higher excitation power. Second, the permanent magnet must be thermally stable (that somewhat contradicts to the previous requirement). Next, the permanent magnet must be transparent for the pulsed field generated by the fast coil and insensitive to this field. Finally, one must take into the account a necessity of fine tuning the field in each gap.

One obvious way of simultaneous tuning the static magnetic field in both gaps is changing the volume of the permanent magnets in the magnetic circuit. To compensate for thermal effects and to adjust field in each gap to remove unwanted resonances (like it was done in [2]), it would be quite desirable to have a "slow" winding for differential tuning of the magnetic field in the gaps or make the gaps adjustable.

Initial (simplified) evaluation of possible approaches to the magnetic circuit design is based on the load line concept, which allows to narrow the permanent magnet material choice. In the magnetic circuit with a permanent magnet and an air gap, the load line of the magnetic material can be described as a slope of a line from the beginning of the coordinate frame ($\mu 0 \cdot H$, B) to the working point ($-\mu 0 \cdot H_m$, B_m), where index "m" refers to the magnetic material:

$$tg\alpha = \frac{-B_m}{\mu 0 \cdot H_m}, \qquad (4)$$

For a thermally stable magnet, this load line must cross the flux density (B) versus magnetic field (H) demagnetization curve above a "knee" that is usually present for most of magnetic materials. The curves without the "knee" can be found for some SmCo materials, e.g. SmCo-2:17 RECOMA 20 material by Precision Magnetics AG [5]. This means that the material is stable in a wide range of temperatures and loads. There are materials with higher saturation magnetization, but we choose this material as a starting point. Besides, there exist thermally compensated alloys made of this material with similar magnetization characteristics that can be employed for building the system. The

residual magnetic flux density of this RECOMA 20 material is Br = 0.9 T and coercive force Hc = 700 kA/m. The magnetization curve is very close to a straight line:

$$B(H) = Br\cdot(H+Hc)/Hc; \quad (5)$$

As follows, B(-Hc) = 0 and B(0) = Br. Effective relative permeability corresponding to this magnetization curve is $\mu = Br/(\mu 0\cdot Hc) \approx 1.02$. High residual magnetization of the material Br allows using relatively thin blocks of the material, which helps to keep the air gap reasonably small. Preliminary estimates show that the thickness of the SmCo insert needed to get 700 Gs flux density in the YIG blocks per Fig. 1 is of the order of several millimeters. This helps to keep the size and power of the fast excitation circuit under control.

While using the fast excitation, another problem needs to be resolved: SmCo 2-17 alloys have specific resistance $\rho \approx 8.6*10^{-7}$ Ohm-m, which can be compared with that of stainless steel. As we saw before, 2-mm stainless steel plate effectively shields the magnetic field in the frequency range of interest. On another hand, it would be great to avoid possible negative effects of penetration of the fast bias magnetic field into the SmCo blocks. High negative magnetic field in the permanent magnet blocks combined with elevated temperature, can result in the appearance of the knee in the demagnetization curve and possible permanent degradation of the magnet. Both issues can be resolved by making the permanent magnet insert consisting of several narrow blocks (thus giving a pass for the fast field to penetrate between the blocks) and by capsulation of these blocks in thin-wall copper shells (thus shielding the blocks from the fast field). Fig. 16 below shows possible approach to the phase shifter permanent bias magnetic circuit design, which is a development of the design in Fig. 1.

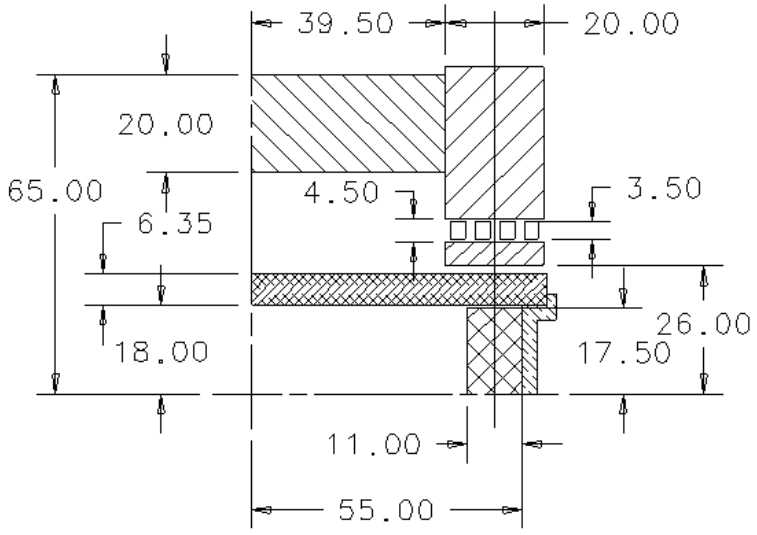

Fig. 16: Permanent bias circuit layout.

Here four permanent magnet blocks, 3 mm wide and 3.5 mm high, are installed in a cartridge (not shown) placed between a pole piece (20 mm wide and 5 mm high) and a vertical flux return slab. This pole piece assembly can move vertically to adjust the gap field, thus providing the needed differential bias tuning. The length of the assembly will

be defined by a required phase shift. At the moment we accept a 200 mm YIG block length as it is shown in Fig. 2.

There are three types of magnetic materials in the circuit. The flux return is made of soft Ni-Zn ferrite G4 by National Magnetics Group [6] with the saturation flux density of ~4600 Gs, residual flux density ~2500 Gs, coercive force ~0.68 Oe, and loss factor $tg\delta/\mu = 10^{-6}$ at 100 kHz and 1 Gs. Saturation curve of the material is shown in Table 5:

Table 5: G4 Saturation Curve

H (Oe)	0	0.2	1	2	5	10	20	100	500
B (T)	0	388	1598	2510	3625	4150	4420	4700	5100
μ	2000	1938	1598	1255	725	415	221	47	10.2

Properties of the permanent magnet material (SmCo-2:17 RECOMA 20 by Precision Magnetics AG [5]) were described earlier. The residual flux density is Br = 0.9 T and the coercive force Hc = 700 kA/m. The magnetization curve is very close to a straight line (5); this implies that the material is stable in a wide range of temperatures and loads. This material is modeled using the constitutive relation $\mathbf{B = \mu 0 * \mu_r * H + B_r}$ with $\mu_r = 1.02$. Another constitutive relation: $\mathbf{B = \mu 0 * (H+M)}$ with M = 716 kA/m can be used with the similar result: the difference in the magnetic field in the YIG block for these two cases is less than 1%. We consider the first case more precise and will use it for modeling.

Properties of the G510 YIG material can also be represented in different ways. First it can be treated as a soft nonlinear material , which can be modeled using a constitutive relation $B = \mathbf{\mu 0 \cdot \mu(B) \cdot H}$. Following magnetization curves provided by the manufacturer, the saturation curve of this material can be presented in a table form, like we did for the G4 flux return material (Table 6):

Table 6: G510 Saturation Curve

H (Oe)	0	0.2	2	10	20	50	100	200	1000	2000
B (Gs)	0	250	426	456	469	501	553	657	1466	2411
μ	1400	1250	213	45.6	23.45	10.02	5.53	3.28	1.47	1.206

Second, a constitutive relation $\mathbf{B = \mu 0 \cdot \mu(B) \cdot H + B_r}$ can be used with $\mathbf{B_r} = 0.0391$ T and "local" (above $\mathbf{B_r}$) relative permeability $\mathbf{\mu(B)}$ defined by the next table:

Table 7: G510 Saturation Curve

H (Oe)	0	0.5	2	10	20	50	100	200	1000	2000
B (Gs)	391	417	437	456	469	501	553	657	1466	2411
μ	60	59	23.2	6.5	3.9	2.2	1.62	1.33	1.07	1.01

In this case, the working point is on the return branch of the magnetization curve, that starts with $\mathbf{B} = \mathbf{B}_r$ at $\mathbf{H} = 0$. The difference in results between the two cases is less than 1.5%. Analysis of the magnetic circuits in Fig. 16 with the chosen magnetization curves results in the magnetic flux density distribution shown in Fig. 17.

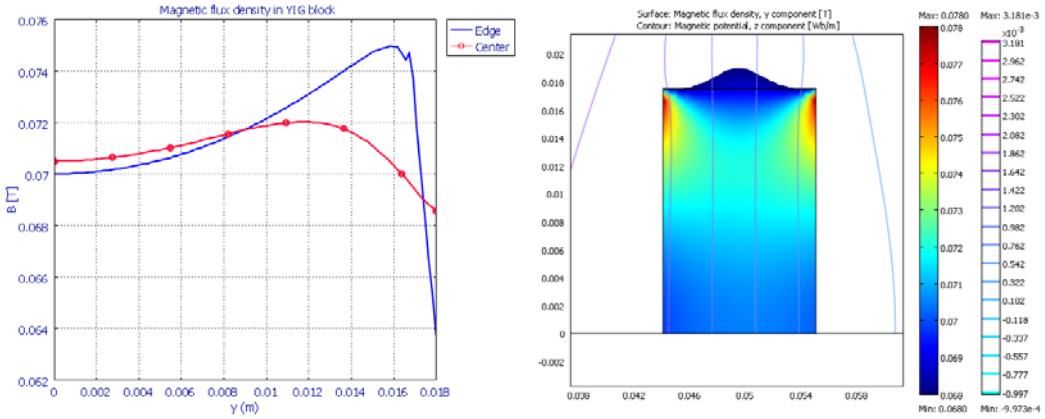

Fig. 17: Flux density distribution in the YIG block

So, there is a solution to the permanent bias field circuit. Now it is time to introduce the pulsed field circuit.

VI. Pulsed Magnetic Circuit

The flux return of the system in Fig. 17 is made of G4 ferrite described above and well suited for use in the frequency range of interest. Aluminum-doped G-510 material by Trans-Tech, Inc (YIG blocks) also behaves as magneto-dielectric.

Because, as it was mentioned before, SmCo is a conductive material, measures must be taken to ensure field penetration through this part of the circuit. As Fig. 16 shows, we have already arranged each permanent magnet section in the magnetic circuit as several separate permanent magnet blocks that can be encapsulated in copper shielding. Gaps between the blocks ensure fast field penetration. Now we need to find requirements for the fast excitation coil. Let's use a safe side approach and request the total phase change of ~150°. This will require a sweep of the magnetic flux density in the YIG blocks from 0.055 to 0.085 T. Let's accept the width of the coils w= 10 mm and the height h= 18 mm and find a current density in the windings that provides the needed flux density change range. Fig. 18 shows that in the static case (DC current), with the ±300 A/mm^2 current density in the winding, we can meet the bias field range requirement.

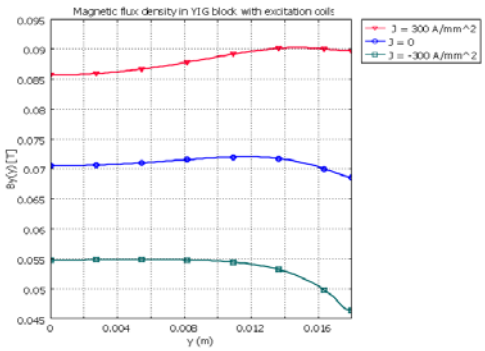

Fig. 18: Magnetic field flux density in the YIG block: DC current.

The magnetic field flux density inside the permanent magnet blocks is quite close to the optimal load line, which crosses the magnetization curve at the point μ0·H = 0.45 T, B = 0.45 T (see Fig. 19 below).

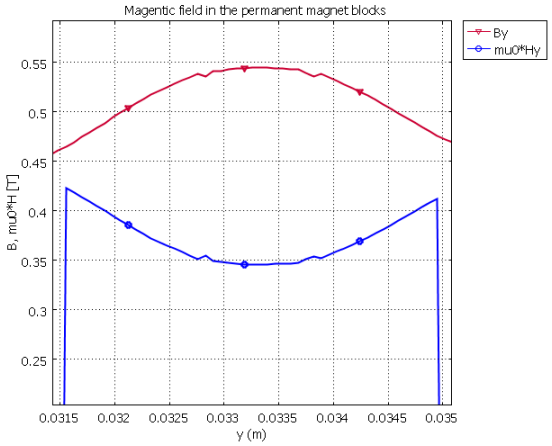

Fig. 19: Magnetic field and flux density in the permanent magnet blocks.

The flux return remains mostly unsaturated even if it carries the maximum magnetic flux. As a result, to simplify further modeling, we can use linear magnetic properties of the flux return material. This simplification does not affect the results we had until this point, and μ = 500 will be used in further modeling. Now we can make another step toward the pulsed circuit modeling. We will introduce high conductivity (e.g. copper) shielding around each permanent magnet block, find the system response to the AC excitation, and then introduce pulsed excitation to complete this stage of the modeling. At this point, we will use another significant simplification by replacing permanent magnets and YIG block with air. Effective permeability of the permanent magnets is 1.03; the YIG blocks are also near saturation: its permeability is ~1.2. Although using this substitute does not help finding the static bias point (we have already found it in the Chapter V) it makes it possible to analyze frequency (or pulse) response of the system.

Let's use 0.5 mm copper shielding around each permanent magnet block and check frequency response of this part of the system. Fig. 20 shows frequency dependence of the magnetic field spatial distribution at 300 A/mm^2 in the area where YIG block is placed

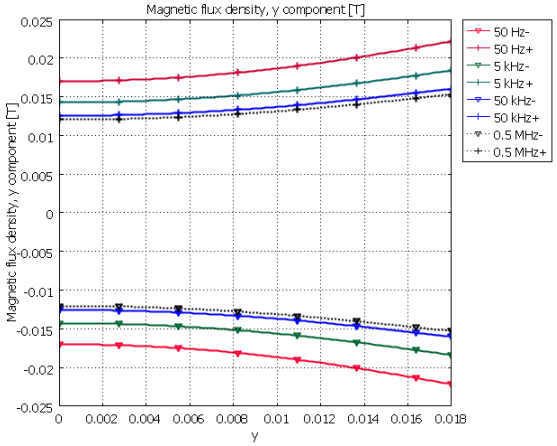

Fig. 20: Achievable flux density change in the YIG blocks at ±300 A/mm^2 in the pulsed excitation windings at different frequencies.

Field swing for each frequency is found as the vertical distance between the corresponding curves separated in phase by 180°. At low frequency, full penetration of the field takes place, and the flux density swing is close to its static value of ±170 Gs. As the field is pushed out of copper with the frequency rise, magnetic resistance of this part of the circuit rises and the effectiveness of the excitation coils becomes lower. This process saturates as the skin layer becomes lower that the thickness of the shielding (only a small difference between f = 50 kHz and 500 kHz exists).

The shielding of the permanent magnet blocks does not lead to a high frequency filtering effect – it only results in some limited increase of the magnetic circuit resistance. To compensate for this increase of the magnetic circuit resistance, we can raise (up to 25%) the excitation current (if needed). On the contrary, as we saw earlier, the horizontal walls of the waveguide have the high frequency filtering effect, preventing the magnetic field from penetrating in the YIG-loaded waveguide.

Now, as we have finalized the geometry of the phase shifter, it is again time to introduce walls of the waveguide into the configuration and find the rise time.
We will use a 5-mm thick side wall made of a hypothetical material with conductivity of $1.25*10^5$ $(Ohm\text{-}m)^{-1}$, which is equivalent to 5 μm thick copper coating from the point of view of eddy current development. Fig. 21 shows the frequency response of this system. As before, the 300 A/m^2 current density was used to generate magnetic field in the area where the YIG block is placed. Magnetic field in a point inside the YIG block is shown against excitation frequency.

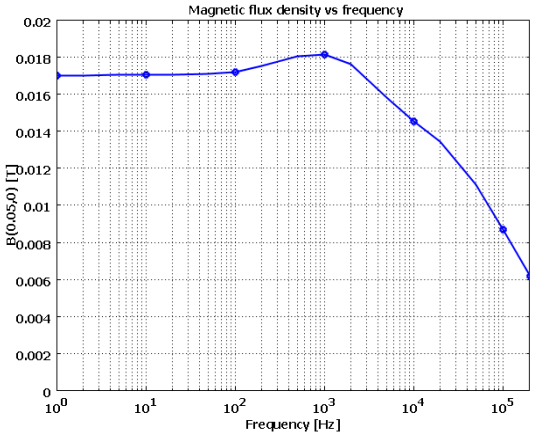

Fig. 21: Frequency response of the system with encapsulated permanent magnet blocks and the waveguide.

This curve should be compared with that in Fig. 14. As we see, the system transparency is quite consistent with that was found earlier. Magnetic field line penetration inside the waveguide is illustrated in Fig. 22 through Fig. 24 below. At 1000 Hz, although we see eddy currents in the copper cells encapsulating the permanent magnet blocks and in the waveguide side wall, magnetic field is almost undisturbed (Fig. 22). The eddy currents are quite skinned at 10000 Hz, but still magnetic field is just weakly deformed (Fig. 23). At 100,000 Hz, significant deformation of the field lines due to eddy currents in the top plate occurs as one can see in Fig. 24. In the right part of this figure, the central part of the system is shown.

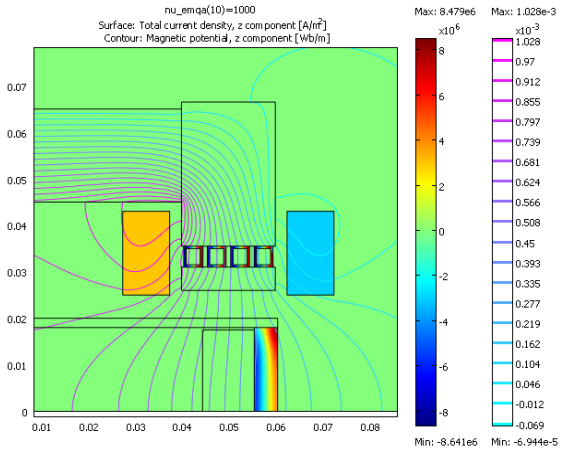

Fig. 22: Magnetic field and eddy currents at 1000 Hz

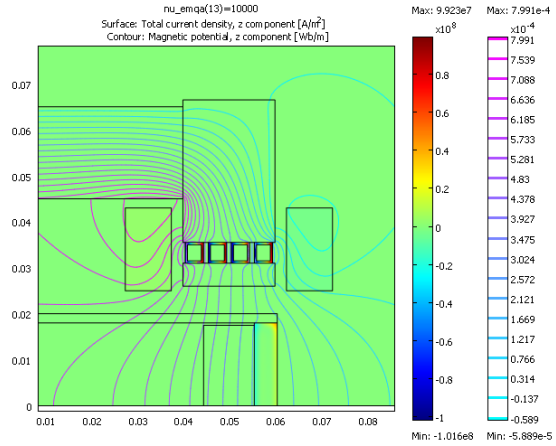

Fig. 23: Magnetic field and eddy currents at 10,000 Hz

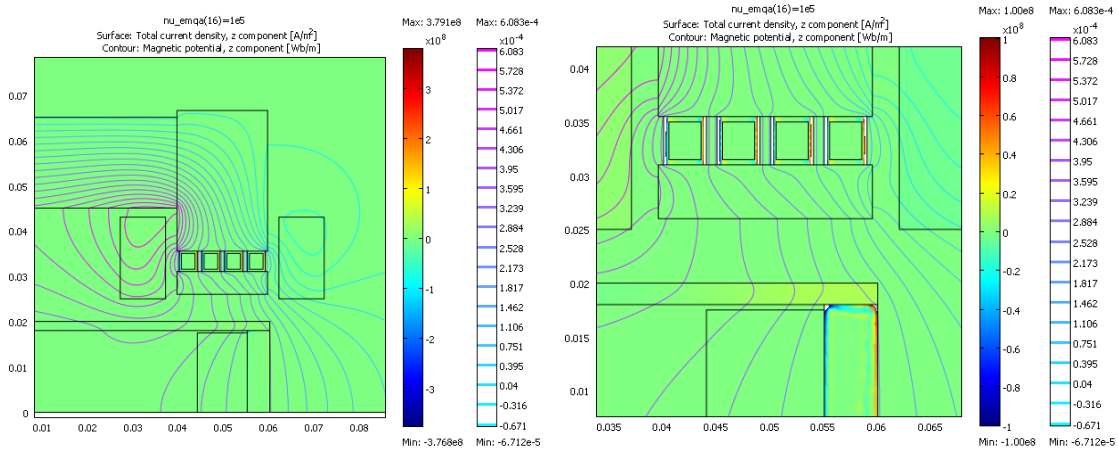

Fig. 24: Magnetic field and eddy currents at 100,000 Hz

In the exercise above, we used a one-turn excitation coil. Although this solution suggests the smallest circuit inductance (or fastest response), it is not practical due to significant complications in the choice of a power supply. Instead, a multi-turn excitation coil must be used with the number of turns optimized from the point of view of getting sufficiently low circuit inductance and current. We will try to configure the circuit that

has 6-turn excitation coil on each pole of the device. With the total current I_{tot} = 600 A, each turn must carry 100 A current.

The impedance of the system is defined by a ratio of the voltage applied to 0.2-meter excitation coil (complex value) to the current in the winding (100 A): $\dot{Z} = \mathring{U}/\omega\dot{I}$. First, let's try to understand how results change depending on the circuit configuration. Table 8 shows parameters of the one-turn circuit as a function of frequency in the case when there is no copper or other conducting material in the air gap of the magnetic circuit.

Table 8: One turn coil parameters as a function of frequency

f (Hz)	10	100	1000	10000	100000
R (mOhm)	0.186	0.243	0.691	2.5	8.8
L (μH)	1.97	1.92	1.75	1.67	1.63
ωL/R	0.67	4.46	15.7	42.5	116

The circuit resistance grows with frequency due to the skin effect and the inductance falls to the limit defined by the fully skinned case. Quality factor ωL/R shows to which extent the circuit has the inductive reaction.

When conductive media is introduces in the circuit (the permanent magnet block encapsulation or waveguide walls), additional power is lost in corresponding elements. This increases the resistive part of the impedance, and reduces the reactive part. The effect is small at low frequency, but makes a serious impact on the system performance at higher frequency. Table 9 demonstrates this by comparing the circuit parameters at 1kHz and 20 kHz before and after the conductive elements are introduced.

Table 9: System parameters with conductors in the magnetic circuit.

	Cu one-turn coil		**Coil + encapsulation**		**Coil + encapsulation + waveguide**	
f (Hz)	1000	20,000	1000	20,000	1000	20,000
R (mOhm)	0.691	3.8	1.4	17.8	1.6	29
L (μH)	1.75	1.65	1.7	1.2	1.67	1.1
ωL/R	15.7	55	7.66	8.5	6.4	4.8

As conducting elements are introduces, the resistive part of the impedance grows and the inductive part becomes smaller. Quality factor is falling down, although we still observe mostly inductive impedance.

In the case of multi-turn coils, the voltage applied to the coil should increase proportionally to the number of turns in the coil (because it is defined by the required flux, which remains the same). Parameters of a 0.2-meter long winding with six turns are presented in the Table 10. Eddy current in the walls of the waveguide, in the magnet encapsulation, and in the turns of the winding were taken into the account here.

Table 10: Circuit parameters for one six-turn 0.2-m long excitation coil

f (Hz)	1000	20,000
R (mOhm)	12.5	225
L (μH)	14	9
ωL/R	6.77	5
U (V) @ 100 A	~10	~120

We see that the quality factor did not change much in comparison with the previous case, so the circuit reaction is mostly reactive. Field lines and current distribution for these two frequencies are shown in Fig. 25.

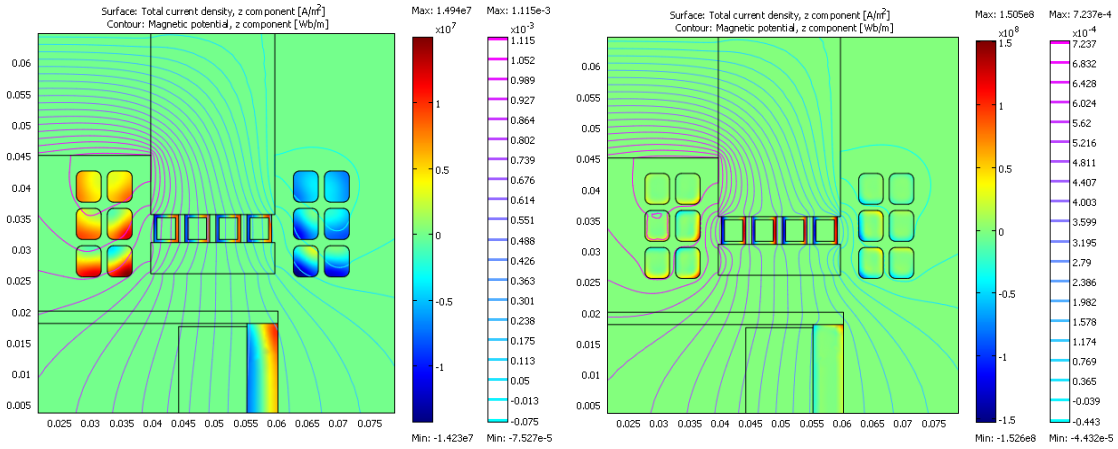

a) b)

Fig. 25: Field lines and current distribution for the six-turn coil system at 1000 Hz (a) and 20,000 Hz (b)

The parameters of the circuits in Table 10 are for one six-turn, 0.2-meter long coil, which presents only one quarter of the system. If to take into the account the whole system with all the turns connected in series, we must multiply all the numbers in the table by four (because with the same current we have four times increase in the stored energy). So, finally, for the 6-turn case with 100 A current, we have the next table:

Table 11: Circuit parameters for the phase shifter excitation system

f (Hz)	1000	20,000
R (mOhm)	50	900
L (μH)	56	36
ωL/R	6.77	5
U (V) @ 100 A	~40	~480

VII. Requirements for a power source

In accordance with the results of the RF modeling in Fig. 7a, and taking into the account the flux density change at the frequency of > 10 kHz in Fig. 20, we can conclude that with the total current swing of 1200 A, the phase change of ~150º is expected. So, the sensitivity of the device to the current change $d\varphi/dI_{tot} = 0.125º/A$. To get a phase ramp rate $d\varphi/dt = 2º/\mu s$, the current ramp rate must be

$$dI_{tot}/dt = (d\varphi/dt) / (d\varphi/dI_{tot}) = 16\ A/\mu s.$$

For a six-turn coil, this translates in the current ramp rate $dI_w/dt = 2.7\ A/\mu s$. Now we can evaluate requirements to a current source. Voltage of a power supply to ensure the needed current ramp rate is $U = L*dI_w/dt \approx 140$ V. The 100 A current and 140 V voltage are well within possible range of parameters of transistor amplifiers.

Besides the inductive part of the bias circuit impedance, the shape of the "voltage – bias" transfer function will depend on the magnetic field diffusion transient properties. In accordance with Fig. 15, we accept time dependent multiplier of this transfer function $K(t) = 1-\exp(-t/\tau)$ with $\tau = 25\ \mu s$. We also accept that the power supply works as the

voltage source before reaching the set current and as the current supply after this (which is a standard arrangement). Then the "voltage-bias" transfer function can be found, which is shown in Fig 26 for power supply voltages 100 V, 200 V, and 500 V. In these graphs, the current rise rate was taken with the inductance of 40 μH, which is close to the data in Table 11.

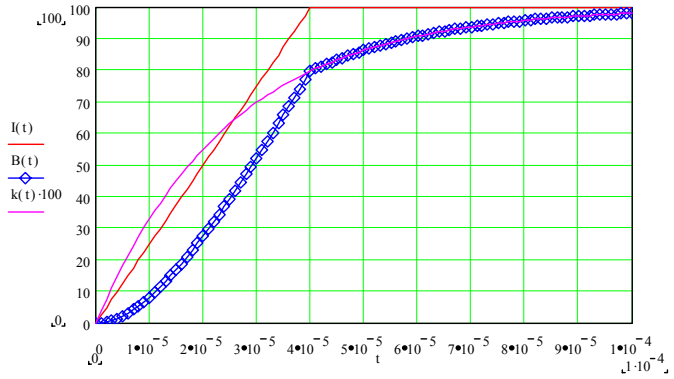

a) V = 100 V

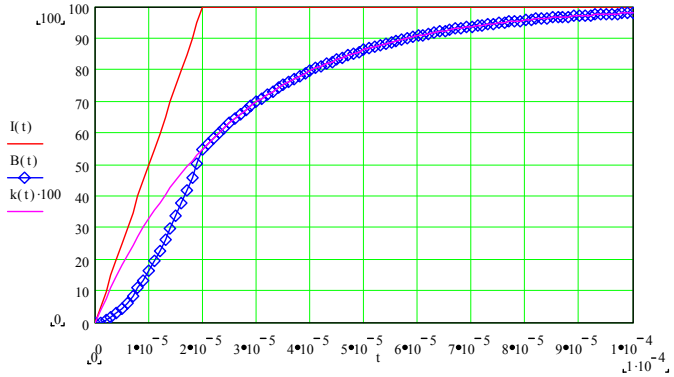

b) V = 200 V

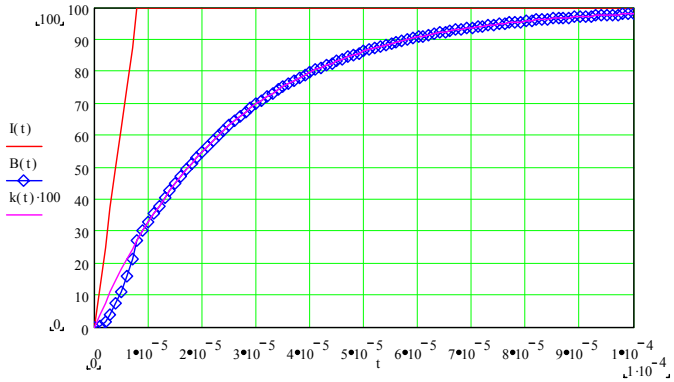

c) V = 500 V

Fig. 26: "Voltage-bias" transfer function of the phase shifter

We can see that, besides the limited field rise time, there is a delay of ~10 μs if a low voltage power supply is used. So, from the point of view of the system performance, it is advantageous to use higher voltage. This issue must be further investigated in the context of the low level RF feedback system.

VIII. Conclusion

As a result of this study, we are able to make the next statements:

1. It is possible to design a phase shifter for a Vector Modulator using YIG block-loaded waveguide so that it can handle power sufficient for feeding standard 1.3 GHz superconducting cavity of a linac:

- It is possible to configure the waveguide to avoid resonances that limit the phase shift range and maximum power
- Maximal temperature rise of the YIG blocks remains quite limited even at rather high RF filling factors

2. It is possible to configure the bias magnetic circuit of the phase shifter using permanent magnets to get to the static working point and fast bias winding for the dynamic bias.

3. It is possible to get the time constant of the device as low as 25 μs.

To complete this development, the next work in the next sequence must be done.

1. Make mechanical design of the device;
2. Order YIG blocks;
3. Order permanent magnet blocks
4. Procure coated ceramic plates
5. Fabricate the waveguide
6. Fabricate the static magnetic circuit
7. Fabricate the fast bias windings
8. Make low power RF measurements
9. Design and fabricates a pulser for fast bias
10. Test fast tuning capabilities of the shifter
11. Test power handling capability of the shifter.
12. Make two phase shifters and configure a Vector Modulator
13. Make RF measurements of the VM performance

Approximate time scale of this activity is ~ 2 years.

IX. References:

1. B. Foster, et al, “High Power Phase Shifter”, Proceedings of 2005 Particle Accelerator Conference, Knoxville, TN, 2005, pp. 3123 – 3125.
2. I. Gonin, et al, “Waveguide-Based Phase Shifter Performance Study” FNAL TD note #TD-08-011, April 2008.
3. Y.W. Kang, et al, “Development and Testing of High Power RF Vector Modulators”, Proceedings of 2007 Particle Accelerator Conference, Albuquerque, NM, 2007, pp. 2508 – 2510.
4. Y. Kang, “Fast Ferrite Phase Shifter for High-Power Applications”, LINAC-XX, Monterey, Ca, 2000, proceedings, pp. 1012 – 1014.
5. http://www.precisionmagnetics.com/pdf/recoma.pdf
6. http://www.magneticsgroup.com/pdf/G4.pdf
7. D. Valuch, High CW Power, Phase, and Amplitude Modulators realized with Fast Ferrite Phase Shifters, PhD Thesis, Slovak University of Technology, Bratislava, 2004.